SSRG International Journal of Applied Physics
ISSN: 2350-0301/ https://doi.org/10.14445/23500301/IJAP-V9I3P102

Volume 9 Issue 3, 19-33, Sep-Dec 2022


*Original Article*

# Design and Construction of Ferrite Based High Sensitive Fluxgate Sensor using Multiple Feedback Band-Pass Filter

Samson Dauda Yusuf[1], Husseini Umar Arafat[2], Jibrin Abdullahi[3]

[1,2]*Department of Physics, Nasarawa State University Keffi, Nigeria.*
[3]*Department of Electrical/Electronic Engineering Technology, School of Engineering Technology, Isa Mustapha Agwai I Polytechnic Lafia, Nasarawa State, Nigeria.*

Received: 02 October 2022 Revised: 06 November 2022 Accepted: 19 November 2022 Published: 02 December 2022

***Abstract*** *- The importance of magnetic sensors in their use to explain some of the complex phenomena relating to geomagnetic storms and solar-terrestrial systems, most of them still have problems of sensitivity, noise level and linearity due to the magnetic material used in designing them. This study developed a ferrite-based, highly sensitive Fluxgate Sensor (FS) for earth's magnetic field explorations using Manganese Zinc (MnZn) ferrite alloy ring core material. The characteristic of the fluxgate sensor was modeled using a trans-impedance operational amplifier and high-quality band-pass filter using multiple feedback band-pass filter MFB-BPF. The result shows that with an optimum core diameter of 12.82mm and excitation current of 25mA, the core was saturated at an excitation frequency of 2kHz with the maximum magnetic field of ±49.44μT (i.e. 4.34V towards the North Pole with corresponding field 49.44μT(49,440nT) and 0.187V towards South Pole with the corresponding field -49.44μT(-49,440nT)) and sensitivity of 87.78mV/μT was realized. The developed FS has reduced sensor dimension, less power consumption, enhanced sensitivity, less noise level and lower fabrication cost, thus meeting the earth's magnetic field studies requirements.*

***Keywords*** *- Fluxgate sensor, Manganese Zinc Ferrite, Multiple feedback, Alloy ring, Operational amplifiers, Magnetic field.*

## 1. Introduction

Fluxgate sensors are commonly used magnetic field sensors for measuring DC or low-frequency AC magnetic field vectors [1]. Earth magnetic field sensors less than 1mT used for low field strength and low-frequency magnetic field with less than 1 kHz used for earth's magnetic field studies include; Anisotropic-Magneto-Resistance (AMR), fluxgate sensor, Giant Magneto-Impedance (GMI), and Giant Magneto-Resistance (GMR) sensors [1]. Traditional Fluxgate Sensor (FS) comprises a ferromagnetic core, wire-wound excitation and pickup coils [2]. They have low noise, high sensitivity, and good sensing accuracy. However, when compared to other competitive magnetic sensors such as Magneto-Impedance (MI) sensors and Magneto-Resistance (MR) sensors etc., the traditional Fluxgate Sensors are larger due to wire-wound coils, more power requirement and less integration capability [1, 2]. Due to developments in system miniaturization, the recent progress in miniature Fluxgate Sensors (FS) with Printed Circuit Board (PCB) and magnetic on Silicon fluxgate (coils replaced with metallic layers and layers interconnections) has been bright [1]. However, they have limitations on the handiness of space; the total number of metallic layers and coil turns will result in higher noise levels and lower sensitivity of the sensors.

Fluxgate sensor design problems usually involve many design variables with multiple objectives under complex non-linear constraints [3]. The sensitivity and noise level of the Fluxgate Sensor depends on the number of windings, the size of the core and the relative permeability of the core material used [4]. The core material causes demagnetization that determines the magnitude of the sensor voltage [5]. It can magnetize with very high permeability (μr ~ 105) [6], less coercivity, and saturation magnetic induction at 550mT [7]. Due to the low power losses of the ferrite alloy, early fluxgate sensors were made-up of ferrite as magnetic core material [8]. However, ferrite-based fluxgate sensors display ill sensor performance due to their low permeability [7]. Precedence literatures concentrated on NiFe permalloy as the magnetic core material because of its high permeability [9]. Yet, the high saturation magnetic flux density and low resistance [10] of iron-nickel led to the outgrowth of Co-based amorphous alloy. The Co-based amorphous alloy soft magnetic material became an ideal substitute for Permalloy due to its high permeability, low coercivity, suitable temperature, and aging stability [11]. Hence, it is widely used in producing fluxgate sensors [12]. High resistance to electricity is suitable in the cores of magnetic field sensors to reduce eddy currents. Square-loop can be magnetized in either of the two directions by an electric current. This

property makes them useful in the memory cores of digital computers since it enables a tiny ferrite ring to store binary bits of information. Records of the earth's magnetic field strength and low-frequency magnetic field disturbances require a small size, highly sensitive, low noise, and stable magnetic field sensor with directional capabilities.

Hence, the objective of this study is to design and construct a ferrite based high sensitive fluxgate sensor using multiple feedback band-pass filters considering the critical parameters of the appropriate commercial-off-the-shelf MnZn ferrite ring core such as high initial magnetic permeability, lower saturation flux density, and high excitation frequency of the magnetic material. The Fluxgate Sensor will be designed using traditional techniques with wire-wound excitation and pickup coils to achieve high sensitivity by employing analytical model equations. The performance responses of the fabricated FS will be evaluated by measuring the sensitivity at different locations to obtain the total earth's magnetic field intensity for each location for comparison with the International Geometric Reference Field standard values.

## 2. Materials and Methods

### 2.1. *Materials*

The materials used for the design and development of the ferrite based high sensitive fluxgate sensor and their specifications include Tektronix TPS 2024B Two Channel Digital Oscilloscope, UT-51 LCR Meter, Tenmars TM-191 Magnetic Field Strength Meter, Tektronix (0-72V, 1.2A) PSW 4721 Programmable DC Power Supply, Bar Magnet, Tektronix 2050 Digital Multi-Meter, Analog Magnetic Compass, 5kHz Testing Board, 0.508mm (SWG 25) wire, 0.361 mm diameter (SWG 30) copper wire, Manganese Zinc (MnZn) ferrite alloy ring, and Vero board.

### 2.2. *Methods*

The method for the realization of the ferrite-based high-sensitive fluxgate sensor using Multiple Feedback Band-pass Filters covers circuit designing, hardware construction and output test analysis.

#### *2.2.1. Design Method*

The design of the ferrite-based high-sensitive fluxgate sensor using a Multiple Feedback Band-pass Filter was carried out in a stage-by-stage method according to the block diagram as shown in Figure 1.

*Frequency Generator Design Method*

Following the work of Ripka [13], this frequency generator is a square wave oscillator designed by using three NOT gates from a CMOS logic chip having three independent inverters (IC 4069BD). The proposed frequency generator circuit is shown in Figure 2.

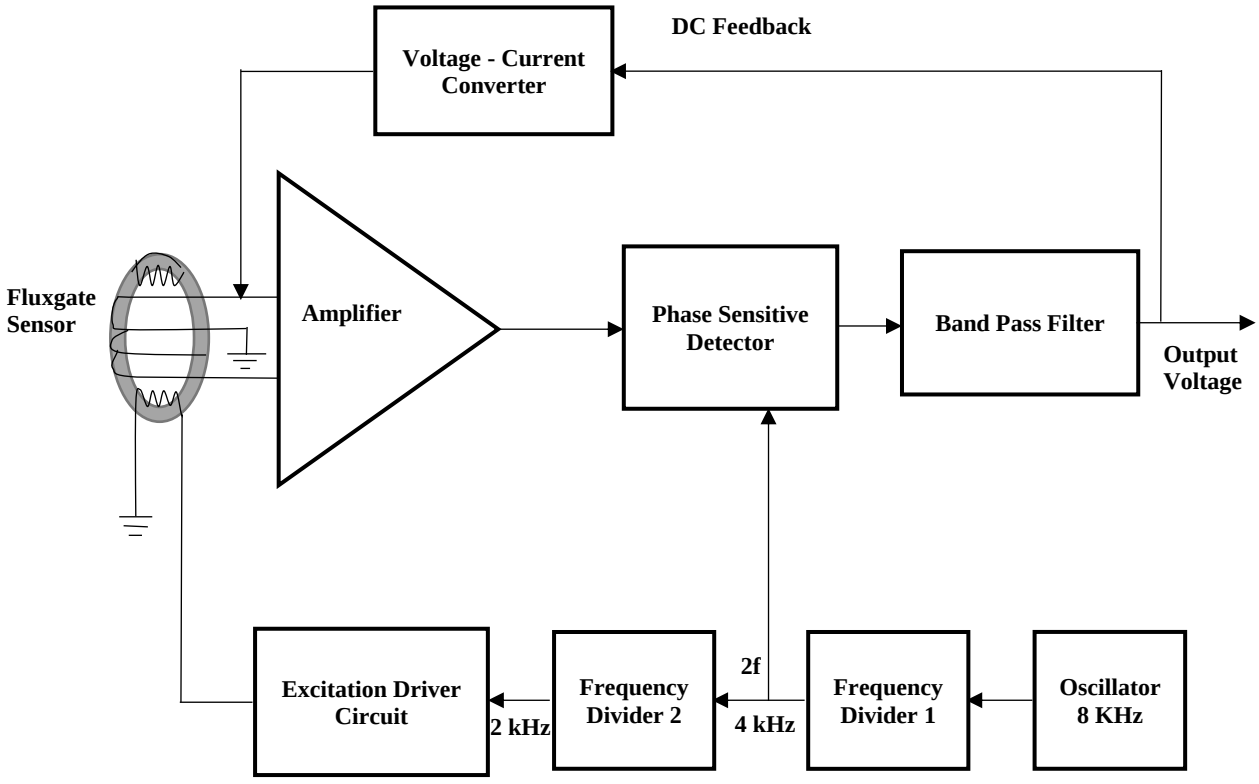


**Fig. 1 Block diagram of the fluxgate sensor**

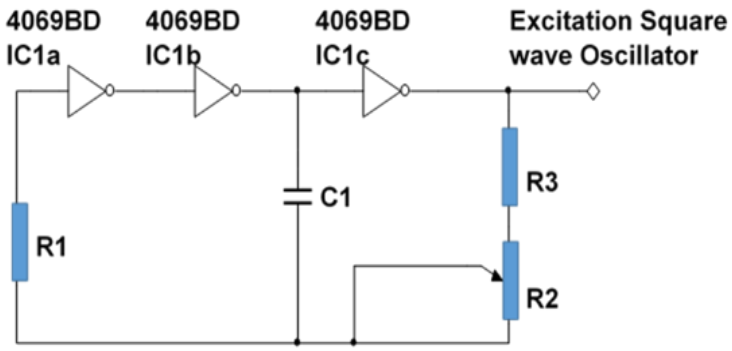


**Fig. 2 Proposed square wave generator stage [13]**

The frequency of the oscillator is determined by the potentiometer $R_2$ fixed resistor $R_3$ and capacitor $C_1$ as defined in the work of Semiconductor [14]:

$$F = \frac{1}{2.2 \times R_x \times C_1} \quad (1)$$

Where F is the frequency in Hz, $R_x$ is the series combination of resistors $R_2$ and $R_3$ in ohms and $C_1$ is the capacitance of the capacitor.

$$R_x = R_2 + R_3 \quad (2)$$

*Frequency Divider Design Method*

The designed frequency divider is a dual-type IC 4013BP; it consists of two flip flops that can be used independently and can divide the incoming square wave frequency into two from the 1.0kHz – 10 kHz oscillator. Following the work of Semiconductor [14], the proposed frequency divider is shown in Figure 3.

*Excitation Drive Design Method*

The frequency divider stage is a voltage-to-current converter stage that produces a weak analog output current, which is insufficient to drive the magnetic core to saturation directly. Hence, the need for current amplification by use of complementary emitter-follower [15]. Following the work of Karthik [16], a low-noise class-AB power amplifier is employed in this study using NPN and PNP transistors Q1 and Q2, respectively, as complementary emitter-follower, as shown in Figure 4. Resistor $R_4$ and diode $D_1$ biased the NPN transistor $Q_1$ while $D_2$ and $R_3$ biased the transistor $Q_2$.

$$\beta = \frac{I_{collector}}{I_{base}} \quad (3)$$

Similarly, the value of the biasing resistors $R_3$ and $R_4$ can be obtained as:

$$R_4 = \frac{V_{cc} - V_{be}}{I_{ref}} \quad (4)$$

Where $R_3$ is equal to $R_4$, $V_{CC}$ is the supplied voltage, $V_{be}$ is the emitter-base voltage, and $I_{ref}$ is the transistor base bias current. Resistors $R_1$ and $R_2$ are equal in values and set the operating current for the output of the transistors. The values of the emitter biasing resistors $R_1$ and $R_2$ are defined as:

$$R_1 = \frac{V}{I_0} \ln\left(\frac{I_{ref}}{I_0}\right) \quad (5)$$

Where $R_1$ is equal to $R_2$, V is the supplied voltage, $I_0$ is the output current, and $I_{ref}$ is the transistor base bias current. The two diodes are to bias the transistors and reduce the cross-over distortion that occurs when the input waveform crosses zero. When the diodes are removed, the oscillator output would have to swing 1.4V to turn one transistor ON and then put the other transistor OFF.

The coupling capacitor $C_1$ blocks the DC component of the current source from reaching the excitation resonant circuit, isolating the AC signal from any DC bias voltages. Thus;

$$C_1 = \frac{1}{3.2 f_{exc} R_{coil}} \quad (6)$$

Where C is the capacitance in Farads, and $f_{exc}$ is the excitation signal frequency in Hertz. $R_{coil}$ is the impedance on the capacitor's load side, which is the excitation coil resistance.

$$F_{exc} = \frac{1}{2\pi R_e C_1} \quad (7)$$

Where $R_e$ is the emitter bias resistor $R_1$, which is also equal to $R_2$ in ohms, while $C_1$ is the output capacitor of the drive circuit in Farad.

When transistor $Q_1$ is turned ON, the capacitor $C_1$ is charged smoothly, as the inductor limits the charging current $L_1$. The inductor $L_1$ limits the current drawn from the source for the fluxgate excitation current.

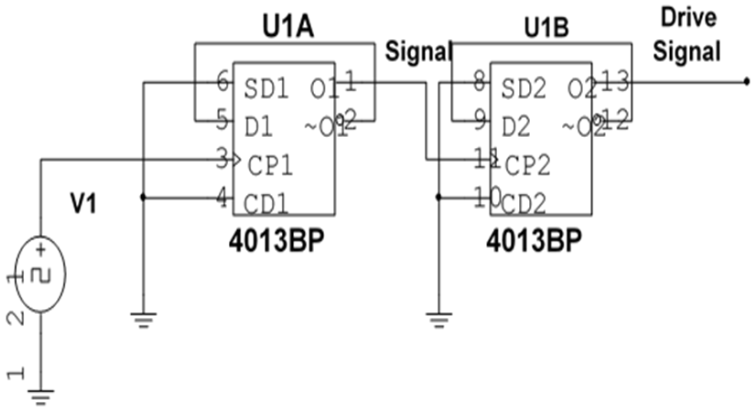


**Fig. 3 Proposed frequency divider stage [14]**

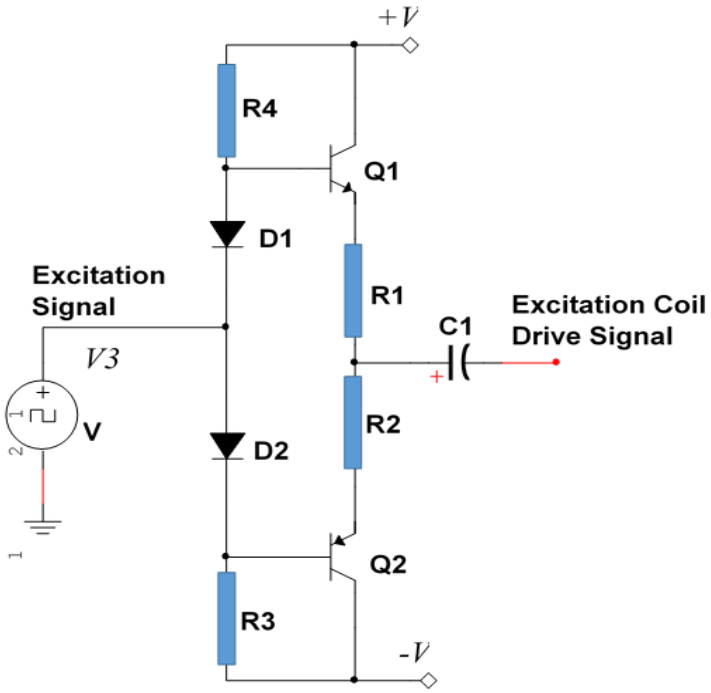


**Fig. 4 Voltage to current converter stage [16]**

*Geometrical Dimensions Design Method*

The ring core material used in this research is Manganese Zinc Ferrite (MnZn) because of its high resistivity, reducing the core's eddy current, low saturation flux density, and high relative magnetic permeability.

The effective cross-sectional area $A_{core}$ of the core material as explained in Core Electronics [17] is:

$$A_{core} = \frac{(d_o - d_i)h_c}{2} \ (m^2) \tag{8}$$

The effective magnetic path length $l_{core}$ as defined by Core Electronics [17] is given as:

$$l_{core} = \frac{\pi(d_o + d_i)}{2} \ (cm) \tag{9}$$

According to Kim *et al.* [18], the right wire size must be considered to prevent the insulation from melting due to Joule heating. Therefore, the number of excitation coil turns $N_{exc}$ is defined as:

$$N_{exc} = \frac{\pi d_i}{d_w} \tag{10}$$

Where, $d_i$ is the inner diameter of the magnetic core and $d_w$ is the winding wire diameter. The inductance $L_{exc}$ of the excitation coil is calculated based on the magnetic

permeability using the equation defined by Core Electronics [17]:

$$L_{exc} = \frac{0.4\pi\mu_c N^2 A_{core}}{l_{eff} \times 10^8} \quad (11)$$

The area of the sensing coil is defined as:

$$A_{sensing} = d_o \times h_c \quad (12)$$

The number of winding turns of the sensing coil depends on the diameter, $d_w$ of the wire that is used, the packing factor $k$ ($k \approx 0.85$ [19]) and the dimensions of the coil [7]. It is defined as:

$$N_{sensing} = \frac{d_o \times h_c}{d_w^2} \quad (13)$$

Sensing coil inductance without the core, as defined by Lundin [20] and Dehmel [19], is:

$$L_{air} = k\frac{\mu_0 N_{sensing}^2 A_{sensing}}{l_{sensing}} \quad (14)$$

Where $k$ is a magnetic field non-uniformity correction factor (also known as Nagaoka's coefficient), Nagaoka's coefficient is generally between 0.7 and 0.95 for pickup coils and always smaller than 1 [19]. The demagnetization factor, as explained in Primdahl [21], Primdahl [22], and Graef *et al.* [23], can be defined as:

$$D_{global} = 0.223\frac{t_{core}}{d_m} \quad (15)$$

Where, $t, d$ and $A_{core}$ imply core thickness, average core diameter and cross-sectional core area, respectively. When the relative permeability, $\mu_r$ and global demagnetization, $D_{global}$ are known, then following the work of Primdahl [21], the apparent permeability, $\mu_a$ is defined as:

$$\mu_a = \frac{\mu_r}{D_{global}(\mu_r - 1) + 1} \quad (16)$$

The inductance of the sensing coil with the core is defined from the expression in Lundin [20] as:

$$L_{sensing} = k\frac{\mu_0 N_{sensing}^2 (A_{sensing} + 2(\mu_a - 1)A_{core})}{l_{sensing}} \quad (17)$$

*Synchronization Switch Design Method*

The PNP transistor and 4066BD quad analog switch were used as synchronization switches due to their low charge injection to avoid offset problems, as shown in Figure 5. To cause the base current to flow in a PNP transistor, the base needs to be more negative than the emitter (current must leave the base) by approximately 0.7 volts for a silicon device or 0.3 volts for a germanium device.

The transistor base current is defined as:

$$I_b = \frac{I_c}{\beta} \quad (18)$$

The value of the input resistor $R_1$ is determined as:

$$R_1 = \frac{V_{ref} - V_{be}}{I_b} \quad (19)$$

Therefore, the value of the load resistor $R_2$ is defined as:

$$R_2 = \frac{+V_s}{I_c} ln\left(\frac{I_b}{I_c}\right) \quad (20)$$

Where $I_b$ is the transistor base current, $I_c$ is the transistor collector current, β is the transistor dc gain, $R_1$ is the base resistor, $R_2$ is the load resistor, $V_{ref}$ is reference signal input voltage, $V_{be}$ is the emitter-base voltage, $V_S$ is the supplied voltage $+V_s$.

*Analog Conditioning Output Design Method*

To produce a DC output voltage proportional to the applied external static (DC) magnetic field and further boost the fluxgate signal, a high-quality factor Q band-pass filter configuration at 5 Hz lower bound and 10 Hz upper bound frequency was designed for experimentation, as shown in Figure 6. Following the work of Evans [24], the Analog conditioning stage of the sensing coil output comprises a coupling capacitor to block the quasi-static feedback current, a trans-impedance amplifier, and a high-quality factor band-pass filter was implemented using an MFB-BPF configuration at 10 Hz frequency.

The sensing coil resonant frequency is obtained based on 2nd, 3rd, 4th, and 5th harmonic frequencies using the equation:

$$f_{2nd} = \frac{1}{2\pi\sqrt{L_{sense}C_{resonant}}} \quad (21)$$

Equation (21) can be rewritten as:

$$C_{resonant} = \frac{1}{(2\pi f_{2nd})^2 L_{sense}} \quad (22)$$

If the gain for the amplifier U1a stage is $G_{U1a}$, the value of the resistor $R_1$, and the value of the feedback resistor $R_2$ is obtained from the amplifier gain formula as:

$$G_{U1a} = \frac{R_2}{R_1} \quad (23)$$

The value of the parallel capacitor $C_1$ will be calculated based on the cut-off frequency $f_0$ given as:

$$f_0 = \frac{1}{2\pi R_2 C_1} \quad (24)$$

$$\therefore C_1 = \frac{1}{2\pi f_0 R_2} \quad (25)$$

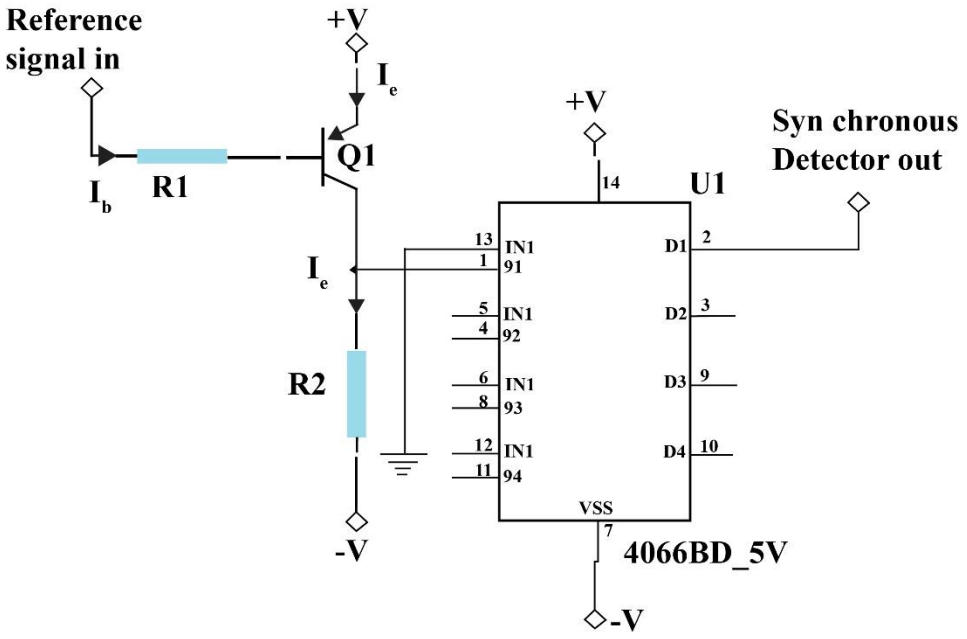


**Fig. 5 Synchronization switch stage [13]**

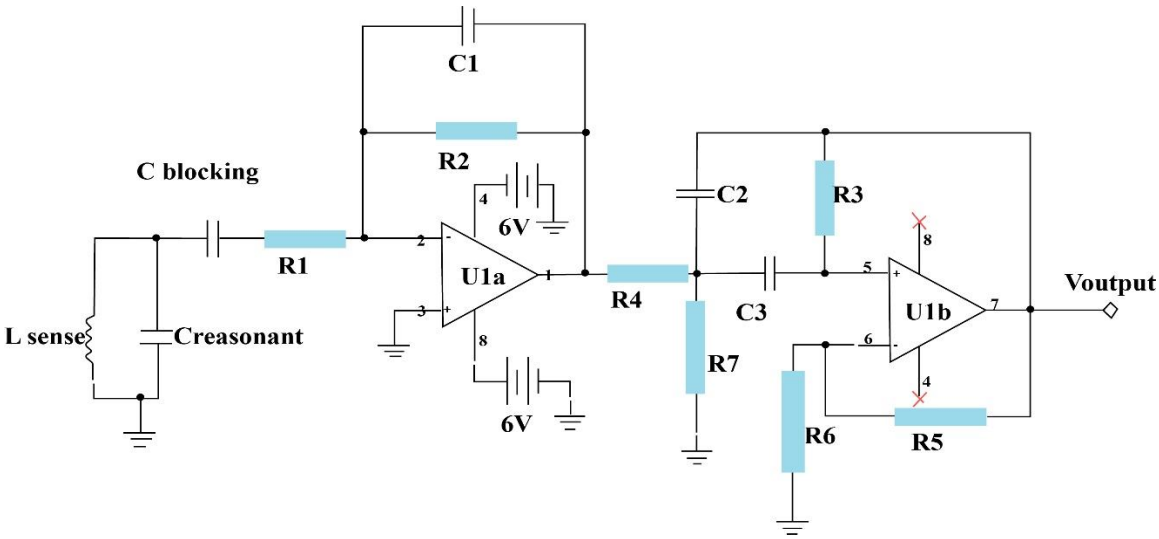


**Fig. 6 Analog conditioning stage of the fluxgate sensor with 2nd order MFB-BPF [24]**

For the second order MFB-BPF, the low-pass filter cut-off frequency is 5Hz, and the high-pass filter cut-off frequency is 10Hz, where the mid frequency is obtained as:

$$f_m = \sqrt{f_l * f_h} \tag{26}$$

The Filter Transfer Function is obtained as follows:

$$\frac{V_0}{V_i} = \frac{-s\left(\frac{1}{R_4C_2}\right)}{s^2 + s\left(\frac{C_2+C_3}{R_3C_2C_3}\right) + \frac{1}{R_3C_2C_3}\left(\frac{1}{R_4}+\frac{1}{R_7}\right)} \tag{27}$$

Filter mid-frequency $f_m$ is given as:

$$f_m = \frac{1}{2\pi} \cdot \sqrt{\frac{1}{R_3C_2C_3}\left(\frac{1}{R_4}+\frac{1}{R_7}\right)} \tag{28}$$

Equation (27) can be reduced to:

$$\frac{V_0}{V_i} = \frac{-G(2\pi f_m)s}{s^2 + 2\varepsilon(2\pi f_m)s + (2\pi f_m)^2} \tag{29}$$

The input resistor $R_4$ is given as:

$$R_4 = \frac{1}{2\omega_m G} \tag{30}$$

The attenuation resistor $R_7$ is given as:

$$R_7 = \frac{1}{\omega_m(2Q - G)} \quad (31)$$

Also, resistor $R_3$ is given as:

$$R_3 = \frac{Q}{\omega_m} \quad (32)$$

Where the pass band gain is given as:

$$G = \frac{R_3}{R_4} . \frac{-C_3}{C_2 - C_3} \quad (33)$$

Considering U1b, the gain resistor $R_6$ describes the gain of the low pass filter as:

$$G = \frac{R_6 + R_5}{R_6} \quad (34)$$

*2.2.2. Hardware Construction Method*

The prototype construction of the Fluxgate Sensor was carried out following the design specifications. The designed circuit prototype was first constructed on a breadboard and later transferred to a Vero board for permanent soldering and packaged in a casing.

*2.2.3. Circuit Testing Method*

The developed FS was then characterized to ascertain its functionality. Accordingly, the excitation coil was excited while the output of the sensing coil was conditioned using an amplifier and the proposed filters. The sensor was exposed to the external and earth's magnetic fields. The excitation coil signal waveforms were examined by connecting the digital signal oscilloscope to the input and output of the sensor excitation stage on the testing board.

The voltage sensitivity $S_{sen}$ of the sensors as defined by Tumanski [7] is given as:

$$S_{sen} = \frac{\text{change in output}}{\text{change in input}}$$

That is,

$$S_{sen} = \frac{dV_{2f}}{dH_{ext}} \quad (35)$$

Where $V_{2f}$ is the second harmonic voltage of the excitation signal and $H_{ext}$ is the external magnetic field. The multiplying factor is defined as:

$$C_{factor} = \frac{Mag_{val}}{V_{tot}} \quad (36)$$

The value of the corresponding voltages for each magnetic field for each component was measured from the relationship:

$$Mag_{val} = C_{factor} \times V_{meas} \quad (37)$$

Where $Mag_{val}$ is the corresponding magnetic field value, $C_{factor}$ is the scale factor, and $V_{meas}$ is the voltage obtained from the fluxgate sensor output during field measurements. All the output voltages obtained from the fluxgate sensor during magnetic field measurements were multiplied by the scale factor to obtain the magnetic field corresponding to the measured output voltages. The total magnetic field intensity, F, obtained by the corresponding earth's magnetic field component at Locations A, B and C is given by:

$$F = \sqrt{X^2 + Y^2 + Z^2} \quad (38)$$

Where X is the Northward magnetic field component, Y is the Eastward magnetic field component, and Z is the downward magnetic field component. Similarly, the measurement accuracy (%) of the magnetic field is defined as:

$$\%\ accuracy = \frac{M_{meas}}{M_{ref}} \times 100\% \quad (39)$$

Where $M_{ref}$ is the IGRF magnetic field standard values and $M_{meas}$ is the total magnetic field values obtained from the magnetic field measurement at different locations (A, B and C) using the developed fluxgate sensor with MFB-BPF.

## 3. Results

### *3.1. Design Analysis*

*3.1.1. Frequency Generator Design Stage*

If the value of the capacitor is chosen to be 2.7nF and the resistor $R_1$ value is 10 kΩ, the maximum frequency of 10 kHz could be achieved when resistor $R_2$ is zero ohms, and only resistor $R_3$ exists. Therefore, the value of resistor $R_2$ is calculated using Equation (1) as:

$$10 \times 10^3 = \frac{1}{2.2 \times R_3 \times 2.7 \times 10^{-9}}$$

$$R_3 = 16.835k\Omega$$

Also, for the minimum frequency of 1.0 kHz, by using the series combination of resistors $R_2$ and $R_3$ the value of the timing resistor $R_x$ is calculated by using Equation (1) as:

$$1.0 \times 10^3 = \frac{1}{2.2 \times R_x \times 2.7 \times 10^{-9}}$$

$$R_x = 168.350k\Omega$$

Since $R_x$ is a series combination of $R_2$ and $R_3$, then from equation (2).

$$R_2 = 168.350k\Omega - 16.835k\Omega = 151.515k\Omega$$

Therefore, resistors $R_1$, $R_2$ and $R_3$ with capacitor $C_1$ are the timing components where the total charge on the

capacitor is proportional to the voltage. Varying the value of the potentiometer resistor $R_3$ will result in changing the output frequency of the oscillator.

*3.1.2. Frequency Divider Design Stage*

The frequency divider is a Dual-type Flip-Flop. Pins D1 & D2 are meant for data input which could be logic 1 or 0. Pins CP1 and CP2 take the clock for Flip Flops 1 & 2. This clock input is of the edge-triggered type, so it switches output states to sudden changes in voltage level. The SD1 and CD1 and SD2 and CD2 are Set and Reset pins of the respective Flip Flops. To connect the IC 4013 as a Frequency divider, the complement pin (~Q) is connected to the data input D1 of the flip flops. The feedback signal of the complement (~Q) pin connected to the data input divides the clock signal frequency of any range by half. Connecting the next Flip flop in such a way gives a signal of F/4 of the original frequency from the square wave oscillator. Thus we can obtain F/8 and F/16 signals by connecting the Flips Flops in continuous sequence [14].

*3.1.3. Excitation Drive Design Stage*

In order to reduce power consumption by the designed sensor and drive the magnetic core into saturation, a 5V power supply is applied to the voltage-to-current converter, with a specified drive current of 25mA. By considering a current gain $\beta$ of 15 and a collector current $I_{collector}$ of 25mA, the base current $I_{base}$ was found from Equation (3) as:

$$15 = \frac{25 \times 10^{-3}}{I_{base}}$$

$$\therefore I_{base} = 1.66mA$$

The values of the biasing resistors $R_3$ and $R_4$ were found using Equation (4): Therefore, by using an emitter-base voltage of 0.7V, the resistor $R_4$ is calculated as:

$$R_4 = \frac{5 - 0.7}{1.66 \times 10^{-3}} = 2.58\ k\Omega$$

Therefore, by considering the excitation frequency of 2 kHz and in order to obtain the right size for the capacitor $C_1$, emitter resistor $R_e$ is chosen to be 15Ω. Hence, capacitor $C_1$ is calculated using Equation (7):

$$2 \times 10^3 = \frac{1}{2 \times 3.142 \times 15 \times C_1}$$

$$\therefore C_1 = 5.3\mu F$$

*3.1.4. Geometrical Dimensions Design*

Assuming the geometrical dimensions of the ferrite ring core are chosen such that that internal radius, $d_i$, is 0.763 cm, outer radius, $d_o$, is 1.282 cm and height, $h_c$, is 0.532 cm, the effective cross-sectional area $\mathrm{A_{core}}$ of the core, the material is calculated using Equation (8):

$$\mathrm{A_{core}} = \frac{(1.282 - 0.762) \times 0.532}{2}\ (\mathrm{cm^2}) = 0.138\mathrm{cm^2}$$

The effective magnetic path length $\mathrm{l_{core}}$ was calculated using Equation (9):

$$\mathrm{l_{core}} = \frac{3.142 \times (1.282 + 0.762)}{2}\ (\mathrm{cm}) = 3.211\mathrm{cm}$$

Considering the wire's demagnetization factor and temperature increase, the wire diameter of 0.508mm Standard Wire Gauge (SWG 25) was chosen as the excitation coil. The inner diameter of the ring is used to determine the number of excitation coil winding as the winding turns used to be denser at the inner diameter than the outside diameter of a ring core. Therefore, the number of excitation coil turns $N_{exc}$was found by using Equation (10):

$$\mathrm{N_{exc}} = \frac{3.142 \times 0.00762}{0.000508}\ \mathrm{turns} = 47\ \mathrm{turns}$$

By using Equation (11), the inductance $L_{exc}$ of the excitation coil is calculated based on the magnetic permeability of 10,000 given as:

$$\therefore L_{exc} = \frac{0.4 \times 3.142 \times 10000 \times 47^2 \times 0.138}{3.211 \times 10^8} = 11.93mH$$

The area of the sensing coil was calculated based on the assumption that the outside diameter and height of the ring core are equal to the length and breadth of the sensing coil using Equation (12):

$$\therefore A_{sensing} = 0.01282 \times 0.00532 = 6.820 \times 10^{-5} m^2$$

By considering sense coil winding capacitance, the wire diameter of 0.361mm Standard Wire Gauge (SWG 30) was chosen as the fluxgate sensing coil. Assuming that the outside diameter forms the winding length, the number of winding layers equals the ring core height. Then using Equation (13), the number of the sensing coil winding turns is calculated as:

$$\therefore \mathrm{N_{sensing}} = \frac{0.01282 \times 0.00532}{0.000361^2} \cong 523\ turns$$

Sensing coil inductance without the core was calculated using Equation (14):

$$\therefore L_{air} = \frac{0.85 \times 1.2568 \times 10^{-6} \times 523^2 \times 6.820 \times 10^{-5}}{0.00532} \cong 1.55mH$$

The demagnetization factor was obtained using Equation (15):

$$\therefore D_{global} = \frac{0.223 \times 0.375}{0.907} \cong 9.22 \times 10^{-2}$$

The apparent permeability, $\mu_a$ was calculated using Equation (16):

$$\therefore \mu_a = \frac{10 \times 10^3}{9.22 \times 10^{-2} \times (10 \times 10^3 - 1) + 1} \cong 10.83$$

Inductance of the sensing coil with core was calculated using Equation (17) as:

$$\therefore L_{sensing} =$$

$$\frac{0.85 \times 1.2568 \times 10^{-6} \times 523^2 \times (6.820 \times 10^{-5} + 19.66 \times 0.138 \times 10^{-4})}{0.01282}$$

$$\cong 7.738mH$$

*3.1.5. Synchronization Switch Design Stage*

Assuming a load current $I_c$ of 10mA and a transistor gain of 50, the base current was found using Equation (18) as:

$$\therefore I_b = \frac{10 \times 10^{-3}}{50} = 2 \times 10^{-4}A$$

The value of the input resistor $R_1$ was found from equation (19), with the assumption that the maximum $V_{ref}$ from the driving stage is 2.5V,

$$\therefore R_1 = \frac{2.5 - 0.7}{2 \times 10^{-4}} = 9.0k\Omega$$

Similarly, the value of the load resistor $R_2$ was calculated from Equation (20) as:

$$\therefore R_2 = \frac{5}{10 \times 10^{-3}} ln\left(\frac{2 \times 10^{-4}}{10 \times 10^{-3}}\right) = 1.956k\Omega$$

The transistor's output is fed to the control pin (pin 1) of the analog switch. This switch will be turned ON and OFF at the rate of the reference frequency being used in the fluxgate sensor design.

*3.1.6. Analog Conditioning Output Design Stage*

The sensing coil resonant frequency was obtained based on the 2nd, 3rd, 4th, and 5th harmonic frequencies of the 2 kHz drive frequency of the MFB-BFs. Using Equation (22), for the second harmonic frequency, when 2f = 4 kHz, the parallel capacitor needed to be connected across the sensing coil to extract the 2nd harmonic frequency signal is:

$$\therefore C_{2nd} = \frac{1}{(2 \times 3.142 \times 4 \times 10^3)^2 \times 7.738 \times 10^{-3}} = 204.5nF$$

For the 3rd harmonic frequency, when 3f = 6 kHz, the parallel capacitor needed to be connected across the sensing coil to extract the 3rd harmonic frequency signal is:

$$\therefore C_{3rd} = \frac{1}{(2 \times 3.142 \times 6 \times 10^3)^2 \times 7.738 \times 10^{-3}} = 90.91nF$$

For the 4th harmonic frequency, when 4f = 8 kHz, the parallel capacitor needed to be connected across the sensing coil to extract the 4rd harmonic frequency signal is:

$$\therefore C_{4th} = \frac{1}{(2 \times 3.142 \times 8 \times 10^3)^2 \times 7.738 \times 10^{-3}} = 51.13nF$$

For the 5th harmonic frequency, when 5f = 10 kHz, the parallel capacitor needed to be connected across the sensing coil to extract the 5th harmonic frequency signal is:

$$\therefore C_{5th} = \frac{1}{(2 \times 3.142 \times 10 \times 10^3)^2 \times 7.738 \times 10^{-3}} = 32.72nF$$

Therefore, the 2nd, 3rd, 4th, and 5th harmonics capacitors needed to extract the corresponding frequency signals are 204.5nF, 90.91nF, 51.13nF, and 32.72nF, respectively.

By using 34dB gain for the amplifier U1a stage and considering the value of the resistor $R_1$ to be 10 kΩ the value of the feedback resistor $R_2$ was calculated using Equation (23) as:

$$\therefore 50 = \frac{R_2}{10 \times 10^3}$$

$$\therefore R_2 = 500\ K\Omega$$

Similarly, the value of the parallel capacitor $C_1$ was calculated based on a 4 kHz cut-off frequency $f_0$ by using Equation (25) as:

$$\therefore C_1 = \frac{1}{2 \times 3.142 \times 4 \times 10^3 \times 500 \times 10^3} = 79.56pF$$

For 2nd order MFB-BPF, the low-pass filter cut-off frequency is 5Hz, and the high-pass filter cut-off frequency is 10Hz, where the mid frequency is calculated using Equation (26) as:

$$\therefore f_m = \sqrt{5 * 10} = 7.07\ Hz$$

By chosen capacitor $C_2$ to be 2.2µF and a voltage gain $G$ of 5 with a mid-frequency of 7.07Hz and a filter quality factor $Q$ of 0.52, the input resistor $R_4$ is calculated using Equation (30) as:

$$\therefore R_4 = \frac{1}{4 * 3.142 * 7.07 * 2.2 \times 10^{-6} * 5} = 1.0231K\Omega$$

Also, the attenuation resistor $R_7$ was calculated using Equation (31) as:

$$\therefore R_7 = \frac{1}{2 * 3.142 * 7.07 * 2.2 \times 10^{-6} * (2 * 0.52 - (-5))} = 1.693k\Omega$$

While the resistor $R_3$ was calculated using Equation (32) as:

$$\therefore R_3 = \frac{0.52}{2*3.142*7.07*2.2\times10^{-6}} = 5.32\ k\Omega$$

Where the pass band gain is known from Equation (33) as:

Using Equation (33), Capacitor $C_3$ was therefore found to be 83.11µF.

Assuming a gain of 5 and a gain resistor $R_6$ is selected to be 4.7kΩ. The feedback resistor $R_5$ for the low pass filter gain is calculated using Equation (34) describes the gain of the filter as:

$$\therefore G = 5 = \frac{4.7\times10^{3}+R_5}{4.7\times10^{3}}$$

$$\therefore R_5 = 18.8k\Omega$$

*3.1.7. Overall Schematic Circuit Diagram*

The input signal to the ADC was filtered to reduce the noise of the designed and developed fluxgate sensor from external sources. The overall schematic circuit diagram for the designed fluxgate sensor with MFB-BPF is shown in Figure 7.

The 2nd order MFB-BPF was used to remove the unwanted frequency components from the sensing coil signal and produced a DC output voltage proportional to the applied external magnetic field.

### *3.2. Construction of Fluxgate Sensor with MFB-BPF*

*3.2.1. Circuit Construction*

The excitation coil was driven by the oscillator range of frequency between 1 kHz to 10 kHz. The inner diameter of the ring was 76.20mm, while the outer diameter was 12.82mm with a 5.32mm core height. Considering the wire's demagnetization factor and temperature increase, the wire diameter of 0.508mm (SWG 25) was chosen as the excitation coil. The coils were wound with 47 turns of excitation coil with consideration for denser winding at the inner diameter than the outside diameter of the ring core. While 523 turns of copper wire with 0.361 mm diameter (SWG 30) were wound on coil bobbin for sensing coil. The fluxgate assembly stages are shown in Figure 8.

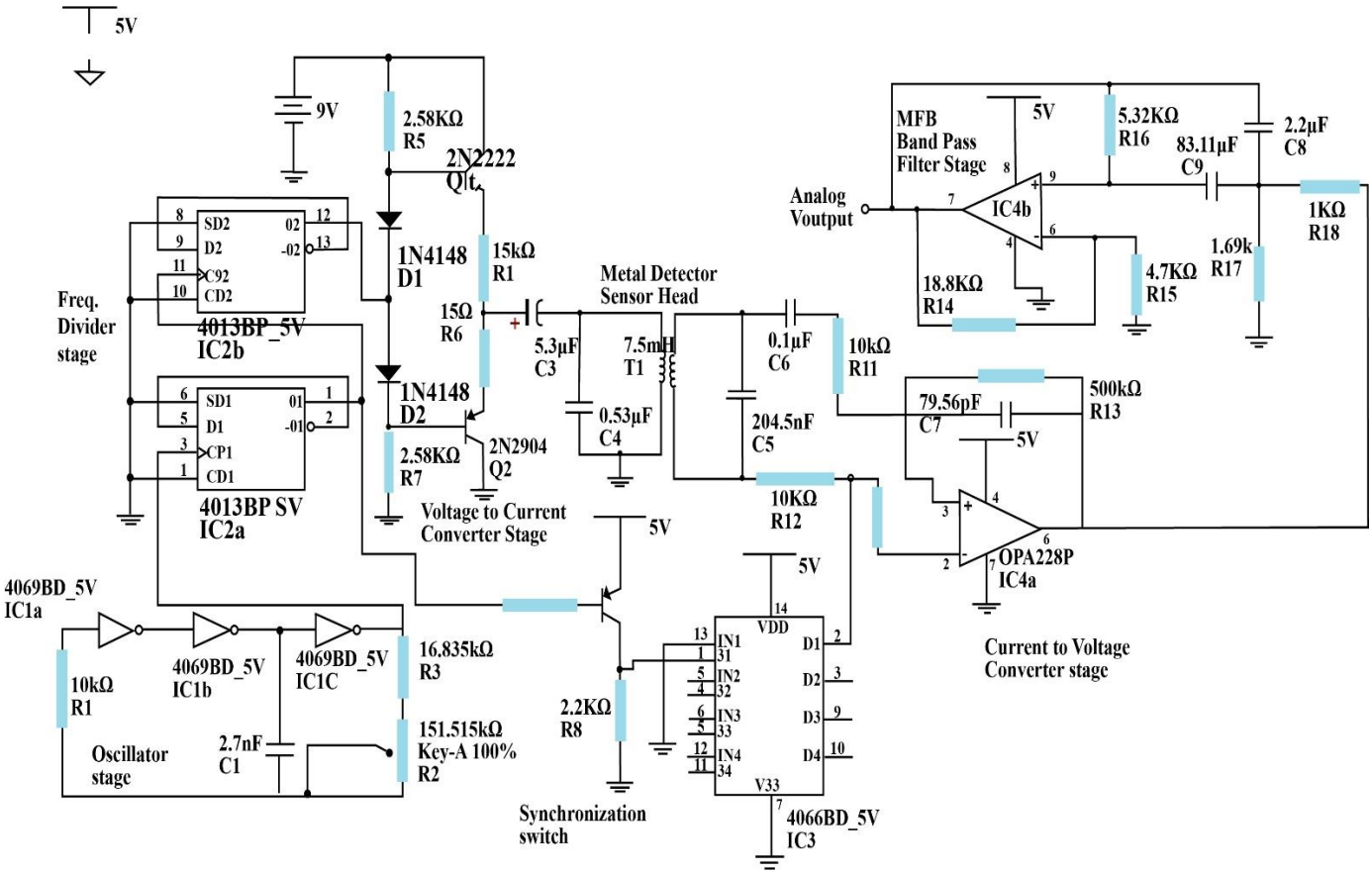


**Fig. 7 Circuit diagram of the designed fluxgate sensor with MFB-BPF**

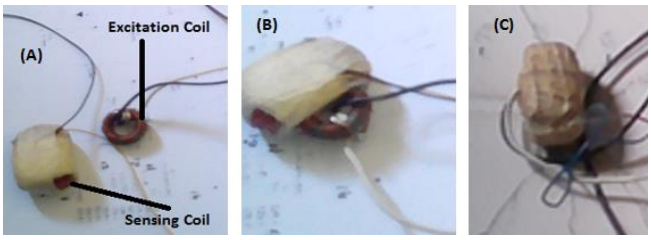


**Fig. 8 Fluxgate Sensor Assembly: (a) Excitation and Sensing (b) Excitation and Sensing coils Coupling and (c) Excitation coil at the Centre of the sensing coil**

*3.2.2. Casing and Packaging*

The constructed fluxgate sensor was provided with a plastic casing for protection measuring 15cm x 12.5cm with 7cm height. It has 3nos. Of 0.5cm diameter holes spaced by 3.75cm for three key switches for backlight, Reset and power. It also has 1no of 7cm x 2.3cm holes for LCD. The isometric diagram of the top and front view of the developed fluxgate sensor casing is shown in Figure 9 (a & b), while the complete casing for the packaged device showing the top and side view is shown in Figure 10 (a & b).

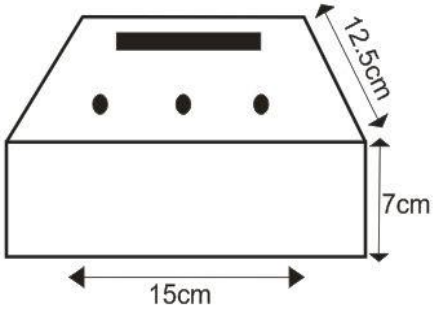


**Fig. 9a Side view isometric diagram of casing**

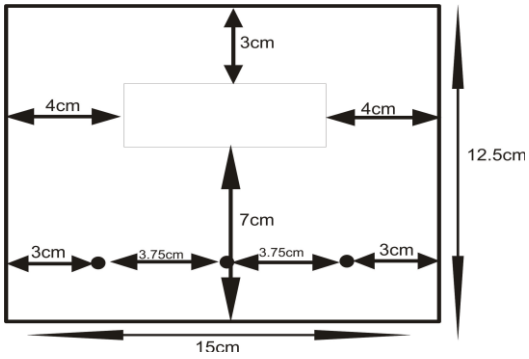


**Fig. 9b Top view isometric diagram of casing**

**Fig. 10a Side view of the complete packaged device**


**Fig. 10b Top view of the complete packaged device**

***3.3. Output Test Analysis***

To evaluate the performances of the developed MFB-based fluxgate sensor, the sensor was exposed to the earth's magnetic field by turning the sensor to 3600 on the horizontal plane. The voltage produced and the magnetic field when the sensor was pointed towards the North Pole, South Pole and East/West were recorded and presented in Table 1.

**Table 1. Magnetic field and output voltage**

| Geomagnetic Components | Output Voltages (V) | Corresponding Magnetic Field Values (nT) |
|---|---|---|
| **North** | 4.34 | 49440 |
| **East/West** | 2.5 | 0 |
| **South** | 0.187 | -49440 |

Since the earth's magnetic field is between 30μT to 50μT [34], the developed fluxgate sensor was therefore considered capable of electronic compasses. The output of the developed fluxgate sensor was clamped to the mean of 2.5V (for 0nT) so that if no magnetic field is present, the output voltage will be 2.5V. Setting this criterion was due to the bi-directional nature of the earth's magnetic field, so 2.5V to 4.34V was allocated for the positive field (towards the North Pole), and 0.187V to 2.5V was for the negative field (towards the South Pole). The magnetic field corresponding to the output voltage is shown in Table 1.

If the second harmonic voltage of the excitation signal $V_{2f}$ is 4.34V, and the external magnetic field $H_{ext}$ is 49.44μT, then the voltage sensitivity $S_{sen}$ of the sensors is calculated using Equation (35) as:

$$S_{sen} = \frac{4.34}{49.44} = 87.78\ mV/\mu T$$

The multiplying factor obtains using Equation (36) as:

$$C_{factor} = \frac{49440.00}{4.34} = 11391.71\ nT/V$$

$$Scale\ factor = 11391.71\ nT/V$$

**Table 2. Output voltages and magnetic fields from an optimized sensor at different locations**

| Earth's Magnetic Field Components | Location A | | Location B | | Location C | |
|---|---|---|---|---|---|---|
| | Voltages (V) | Magnetic Field (nT) | Voltages (V) | Magnetic Field (nT) | Voltages (V) | Magnetic Field (nT) |
| X-Component | 2.990 | 34061.21 | 2.967 | 33799.20 | 2.929 | 33366.318 |
| Y-Component | 0.018 | 205.05 | 0.019 | 216.4424 | 0.024 | 273.40 |
| Z-Component | 0.114 | 1298.65 | 0.155 | 1765.715 | 0.335 | 3816.22 |

For the possibility of using the developed sensor for measuring the earth's magnetic field, the sensor was used to measure the magnetic field at different geomagnetic locations. The earth's magnetic field consists of three components: the vertical component (called Z-component) and the two horizontal components (called X and Y-components). Since, according to Ali *et al.* [26], the earth's magnetic field exist everywhere, the magnetic field corresponding to the output voltages measured for each magnetic field component at the selected locations were calculated using Equation (37). For location A the calculated magnetic fields for the X, Y and Z –components are:

$$Mag_{a(X)} = 11391.71 \times 2.990 = 34061.21\ nT$$

$$Mag_{a(Y)} = 11391.71 \times 0.018 = 205.05\ nT$$

$$Mag_{a(Z)} = 11391.71 \times 0.114 = 1298.65\ nT$$

A similar method was used to calculate the magnetic field components for locations B and C. The results of the output voltages and the corresponding magnetic fields measured at different geomagnetic locations are presented in Table 2.

The total magnetic field intensity, F, was calculated using Equation (38) as:

$$F_a = \sqrt{34061.21^2 + 205.05^2 + 1298.65^2}$$

$$= 34086.5745\ nT$$

$$F_b = \sqrt{33799.20^2 + 216.4424^2 + 1765.715^2}$$

$$= 33845.98\ nT$$

$$F_C = \sqrt{33366.318^2 + 273.40^2 + 3816.22)^2}$$

$$= 33584.9588\ nT$$

The result of the corresponding calculated earth's magnetic field intensity at the three geomagnetic locations is compared with the total magnetic field strength obtained from the International Geomagnetic Reference Field (IGRF) and presented in Table 3. The device's accuracy was also calculated using Equation (39); the results are also presented in Table 3. Thus;

$$\%\ accuracy_a = \frac{34086.5745}{34067.50} \times 100\% = 99.998\%$$

$$\%\ accuracy_b = \frac{33845.98}{33852.70} \times 100\% = 99.98\%$$

$$\%\ accuracy_c = \frac{33584.9588}{33592.90} \times 100\% = 99.976\%$$

**Table 3. Comparison of magnetic fields from IGRF with prototype fluxgate sensor**

| Parameters | Total Magnetic Field Intensity Values | | |
|---|---|---|---|
| | Location A | Location B | Location C |
| FS Total Magnetic Field Intensity, F | 34086.57 | 33845.98 | 33584.96 |
| IGRF Standard Mag. Field intensity, F | 34067.50 | 33852.70 | 33592.90 |
| Measurement accuracy (%) | 99.99 | 99.98 | 99.98 |

From Table 3, the total magnetic field intensity results using the developed fluxgate sensor are comparable with the IGRF Standard.

An accuracy of 99.99% for locations A, B, and C, respectively, validates the possibility of using the developed fluxgate sensor for earth's magnetic field exploration like a compass. The performance of the designed and developed MFB-BPF-based fluxgate sensor in this study was compared with previous work done by other researchers on fluxgate sensors, such as Can and Topal [27], Schoinas et al. [28], and Miles et al. [29] and the result is presented in Table 4. The voltage sensitivity, magnetic field magnitude, excitation current, and sensor core diameter of the present study compared with previous research are presented in Figure 11.

From Table 4, the present study has a smaller sensor core size (diameter) as compared to the optimum core diameter suggested in the solutions reported by Can and Topal [27], Schoinas et al. [28], and Miles et al. [29].

**Table 4. Comparison of current work with some existing fluxgate sensors**

| Reference | Core Diameter (mm) | Max. B (±μT) | Excitation Frequency (kHz) | Excitation Current (mA) | Sensitivity (mV/μT) | Core Material |
|---|---|---|---|---|---|---|
| **Can & Topal [27]** | 20.00 | 60 | n/a | 2.17 | 11.40 | Cobalt Metglas 2714A |
| **Schoinas *et al.* [28]** | 15.00 | 40 | 100 | 300 | 25.00 | Vitrovac 6025 Z |
| **Miles *et al.* [29]** | 26.98 | n/a | 5.0 | 800 | n/a | Permalloy |
| **Present Study** | 12.82 | 49.44 | 2.0 | 25 | 87.78 | MnZn Ferrite |

Lower excitation frequency as compared to Schoinas et al. [28] and Miles et al. [29] due to reduced core dimension, which has resulted in the demagnetization effect of the core, thereby reducing excitation current and hence the power consumption. Higher voltage sensitivity than the sensors reported in Can and Topal [27] and Schoinas et al. [28]. The optimum dimension and geometry of the sensor core, sensing coil, and detection circuit significantly enhanced the voltage sensitivity by a factor of 7.7 due to the matching of the excitation and detection circuits aided by the MFB-BPF employed in this research. A much simpler realization of the ferromagnetic core concerning Can and Topal [27], Schoinas et al. [28], and Miles et al. [29] due to the reduction of the sensor core and the BPF designed without sacrificing precision or size of the sensor.

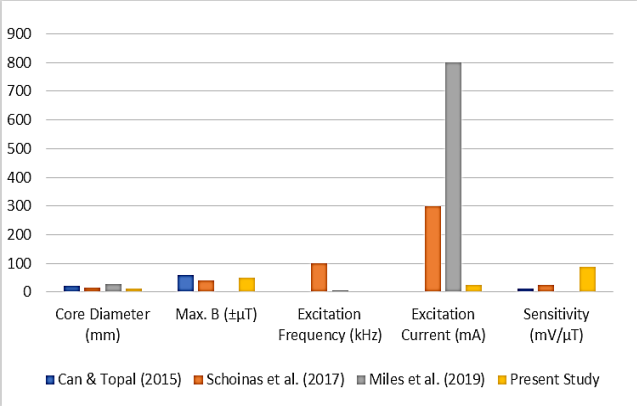


**Fig. 11 Comparison of the present study with previous ones**

## 4. Discussion

The designed fluxgate sensor with MFB-BPF has been carried out using a MnZn Ferrite core material, and the designed sensor, when subjected to various test, have revealed vital information. Findings have shown from this study that the second harmonic voltage of the excitation signal for the designed fluxgate sensor is 4.34V, and the external magnetic field is 49.44μT, corresponding to the sensor's voltage sensitivity of 87.78mV/μT. The high sensitivity results from reduced care diameter, reduced excitation current, and increased magnetic field. This finding is not in line with Can and Topal [27], who designed a ring core fluxgate magnetometer as an attitude control sensor for low and high-orbit satellites and obtained a voltage sensitivity of 11.4mV/μT using a Cobalt-based Metglas 2714A core material. This finding is also not in line with that of Schoinas et al. [28], who worked on a flexible pad-printed fluxgate sensor and obtained a voltage sensitivity of 25mV/μT using a Vitrovac 6025 Z core material.

Findings from this study have also shown that the designed fluxgate sensor with MFB-BPF, when used to measure the earth's magnetic field at different geographical locations, has produced satisfactory results with an accuracy of 99.99% compared with the IGRF Standard. It implies that the developed fluxgate sensor can be used for earth's magnetic field exploration and also as a compass in line with that of Tarnriseven et al. [30], Schoinas et al. [28], and Topal et al. [31], but not similar to that of Douglass et al. [32].

## 5. Conclusion

The developed Fluxgate Sensor has a smaller core size, lower power consumption and excitation frequency due to reduced core dimension, which resulted in the demagnetization effect of the core, thereby reducing the excitation current and the power consumption. The higher voltage sensitivity was achieved as a result of matching the excitation and detection circuits aided by the MFB-BPF employed in the design, and the simple realization of the Ferro-magnetic core was due to the reduction of the sensor core size and BPF design without sacrificing precision. Considering the improved performance of the FS using a trans-impedance amplifier and MFB-BPF, the developed FS achieved the research objective because of its reduced power consumption, enhanced sensitivity, and low cost with efficient fabrication.

## Funding Statement

This study did not receive any specific grant from the public, commercial, or not-for-profit funding agencies.

## References

[1] C. C. Lu, and J. Huang, "A 3-Axis Miniature Magnetic Sensor Based on a Planar Fluxgate Magnetometer with an Orthogonal Flux Guide," *Sensors*, vol. 15, no. 6, pp. 14727-14744, 2015. Crossref, https://doi.org/10.3390/s150614727

[2] J. Z. Tseng, C. C. Wu, and C. L. Dai, "Modeling and Manufacturing of a Micro-Machined Magnetic Sensor Using the CMOS Process without Any Post-Process," *Sensors*, vol. 14, no. 4, pp. 6722–6733, 2014. Crossref, http://dx.doi.org/10.3390/s140406722

[3] O. W. Oluyombo, A. M. S. Tekanyi, S. M. Sani, and B. Jimoh, "Improvement of Sensitivity and Noise of a Fluxgate Magnetometer Using Modified Firefly Optimization Algorithm," *International Journal of Engineering Research & Technology (IJERT),* vol. 6, no. 4, pp. 32-37, 2017. Crossref, https://doi.org/10.17577/IJERTV6IS040104

[4] H. Lv, and S. Liu, "Research on Mems Technology of Micro Fluxgate Sensor," *International Journal of Digital Content Technology and Its Applications (JDCTA),* vol. 7, no. 6, pp. 1159-1167, 2013. Crossref, https://doi.org/10.4156/JDCTA.VOL7.ISSUE6.132

[5] C. Coillot, J. Moutoussamy, G. Chanteur, P. Robert, and F. Alves, "On-Board Hybrid Magnetometer of Nasa Charm-II Rocket: Principle, Design and Performances," *Journal of Sensors and Sensors System,* vol. 2, no. 2, pp. 137–145, 2013. Crossref, http://dx.doi.org/10.5194/jsss-2-137-2013

[6] C. Li, and W. Ren, "Application of Angle and Fluxgate Sensor Algorithm in Designing the Smart Sensor System," *Journal of Chemical and Pharmaceutical Research,* vol. 6, no. 6, pp. 760-767, 2014.

[7] S. Tumanski, "Modern Magnetic Field Sensors. A Review," *Przegląd Elektrotechniczny,* vol. 89, no. 10, pp. 1-12, 2013.

[8] G. Musmann, and Y. Afanassiev, *Fluxgate Magnetometers for Space Research*. Norderstedt: Books on Demand GmbH, pp. 13-24, 2010.

[9] D. He, and M. Shiwa, "A Magnetic Sensor with Amorphous Wire," *Sensors,* vol. 14, no. 6, pp. 10644-10649, 2014. Crossref, https://doi.org/10.3390%2Fs140610644

[10] C. C. Lu, J. Huang, P. K. Chiu, S. L. Chiu, and J. T. Jeng, "High-Sensitivity Low-Noise Miniature Fluxgate Magnetometers Using a Flip Chip Conceptual Design," *Sensors,* vol. 14, no. 8, pp. 13815-13829, 2014. Crossref, http://dx.doi.org/10.3390/s140813815

[11] P. Frydrych, R. Szewczyk, and J. Salach, "Magnetic Fluxgate Sensor Characteristics Modeling Using Extended Preisach Model," *Proceedings of the 15th Czech and Slovak Conference on Magnetism, Kosice, Slovakia*, vol. 126, no. 1, pp. 18-19, 2014. Crossref, https://doi.org/10.12693/APHYSPOLA.126.18

[12] E. Matandirontya, R. Van Zy, D. J. Gouws, and E. F. Saunderson, "Evaluation of a Commercial-Off-the-Shelf Fluxgate Magnetometer For Cubesat Space Magnetometry," *Journal of Small Satellites,* vol. 2, no. 1, pp. 133-146, 2013.

[13] P. Ripka, *Magnetic Sensors and Magnetometers* (2nd Ed.), Boston. Usa: Artech House, pp. 54-78, 2001.

[14] F. Semiconductor, *Cd4049 Hex Inverting Buffer Manual*, Fairchild Semiconductor Corporation, pp. 8-12, 2002.

[15] P. Ripka, "Advances In Fluxgate Sensors," *Sensors and Actuators A: Physical,* vol. 106, no. 1-3, pp. 8–14, 2003. Crossref, https://doi.org/10.1016/S0924-4247(03)00094-3

[16] P. Karthik, "*A CMOS Analog Front-End Circuit for Micro-Fluxgate Sensors,"* M.Sc. thesis, Department Electrical Engeering, Arizona State University, Arizona, Usa, 2013.

[17] Core Electronics, "Vietnam Singapore Industrial Park 2. (1) 3 – 6," 2008. [Online]. Available: http://www.emicore.co.kr/neowiz/img_home/core_all_catalog.pdf.

[18] S. J. Kim, B. Y. Moon, Y. K. Chang, and H. S. Oh, "Design of a Low-Cost 2-Axes Fluxgate Magnetometer for Small Satellite Applications," *Journal of Astronomical & Space Science,* vol. 22, no. 1, pp. 35-46, 2005. Crossref, http://dx.doi.org/10.5140/JASS.2005.22.1.035

[19] G. Dehmel, "Magnetic Field Sensors: Induction Coil (Search Coil) Sensors," *Sensors Set: A Comprehensive Survey,* vol. 5, no. 1, pp. 205–253, 1989. Crossref, https://doi.org/10.1002/9783527620166.ch6

[20] R. Lundin, "A Handbook Formula for the Inductance of a Single-Layer Circular Coil," *Proceedings of the IEEE,* vol. 73, no. 9, pp. 1428-1429, 1985. Crossref, https://doi.org/10.1109/PROC.1985.13304

[21] F. Primdahl, "The Fluxgate Magnetometer," *Journal of Physics E, Science and Instrumentation,* vol. 12, no. 4, pp. 241–253, 1979. Crossref, https://doi.org/10.1088/0022-3735/12/4/001

[22] F. Primdahl, Peter Brauer, José M G Merayo and Otto V Nielsen, "The Fluxgate Ring-Core Internal Field," *Measurement Science Technology,* vol. 13, no. 8, pp. 1248, 2002. Crossref, https://doi.org/10.1088/0957-0233/13/8/312

[23] M. De Graef, and M. Beleggia, "The Fluxgate Ring-Core Demagnetizing Field," *Journal of Magnetism and Magnetic Materials,* vol. 305, no. 2, pp. 403-409, 2006. Crossref, https://doi.org/10.1016/j.jmmm.2006.01.111

[24] K. Evans, "Fluxgate Magnetometer Explained," Invasens, 2006. [Online]. Available: http://www. https://www.invasens.co.uk/FluxgateExplained.PDF

[25] Satyabrata Podder, Paulam Deep Paul, Arunabha Chanda, "The Effect of the Magnetic Field of High Intensities on Velocity Profiles of Slip Driven Non-Newtonian Fluid Flow Through the Circular, Straight Microchannel," *International Journal of Engineering Trends and Technology*, vol. 70, no. 4, pp. 383-388, 2022. Crossref, https://doi.org/10.14445/22315381/IJETT-V70I4P233

[26] A. S. Ali, S. Siddharth, Z. Syed, and N. El-Sheimy, "Swarm Optimization-Based Magnetometer Calibration for Personal Handheld Devices," *Sensors,* vol. 12, no. 9, pp. 12455-12472, 2012. Crossref, https://doi.org/10.3390/s120912455

[27] H. Can, and U. Topal, "Design of Ring Core Fluxgate Magnetometer as Attitude Control Sensor for Low and High Orbit Satellites," *Journal of Superconductivity and Novel Magnetism,* vol. 28, no. 3, pp. 1093-1096, 2015. Crossref, http://dx.doi.org/10.1007/s10948-014-2788-5

[28] S. Schoinas, A. M. E. Guamra, F. Moreillon, and P. Passeraub, "A Flexible Pad-Printed Fluxgate Sensor," *Multidisciplinary Digital Publishing Institute Proceedings*, vol. 1, no. 4, pp. 615, 2017. Crossref, http://dx.doi.org/10.3390/proceedings1040615

[29] D. M. Miles, M. Ciurzynski, D. Barona, B. B. Narod, J. R. Bennest, A. Kale, M. Lessard, D. K. Milling, J. Larson, and I. R. Mann, "Low-Noise Permalloy Ring-Core for Fluxgate Magnetometers," *Geoscience Instrumentation, Methods and Data Systems*, vol. 8, no. 2, pp. 227-240, 2019. Crossref, https://doi.org/10.5194/gi-8-227-2019

[30] S. Tanriseven, H. Can, C. Birlikseven, and U. Topal, "Highly Sensitive Reliable Fluxgate Magnetometer Implementation," Research Gate, 2015. [Online]. Available: https://www.researchgate.net/profile/Sercan-Tanriseven/publication/283725155_Highly_Sensitive_Reliable_Fluxgate_Magnetometer_Implementation/links/5645984f08ae9f9c13e5f60a/Highly-Sensitive-Reliable-Fluxgate-Magnetometer-Implementation.pdf

[31] U. Topal, H. Can, O. M. Çelik, A. Narman, M. Kamiş, V. Cıtak, C. Demet, S. Huseiyin, and P. Svec, "Design of Fluxgate Sensors for Different Applications from Geology to Medicine," *Journal of Superconductivity and Novel Magnetism*, vol. 32, pp. 839-844, 2019. Crossref, https://doi.org/10.1007/s10948-018-4781-x

[32] G. M. Douglas, I. A. Hector, I. Perez, A. F. R. Paulo, A. P. Guillherme, C. C. B. Luiz, W. andre, M. F. Gustavo, G. U. G. Luis, and F. M. C. Mario, "Autonomous Aeromagnetic Surveys Using a Fluxgate Magnetometer," *Sensor*, vol. 16, no. 12, pp. 2169, 2016. Crossref, https://doi.org/10.3390%2Fs16122169

[33] C. C. Lu, and J. Huang, "A 3-Axis Miniature Magnetic Sensor Based on a Planar Fluxgate Magnetometer with an Orthogonal Flux Guide," *Sensors*, vol. 15, no. 6, pp. 14727-14744, 2015. Crossref, https://doi.org/10.3390/s150614727